Cerebral Cortex, September 2017;27: 4361–4378

doi: 10.1093/cercor/bhw239
Advance Access Publication Date: 13 August 2017
Original Article

ORIGINAL ARTICLE

Asymmetric Direct Reciprocal Connections Between Primary Visual and Somatosensory Cortices of the Mouse

Ian O. Massé, Stéphanie Ross, Gilles Bronchti, and Denis Boire

Département d'anatomie, Université du Québec à Trois-Rivières, Canada G9A 2W7

Address correspondence to Denis Boire PhD, Département d'anatomie, Université du Québec à Trois-Rivières, 3351, boulevard des Forges, C.P. 500, Trois-Rivières, Québec, Canada G9A 5H7. Email: denis.boire@uqtr.ca

Abstract

Several studies show direct connections between primary sensory cortices involved in multisensory integration. The purpose of this study is to understand the microcircuitry of the reciprocal connections between visual and somatosensory cortices. The laminar distribution of retrogradely labeled cell bodies in V1 and in the somatosensory cortex both in (S1BF) and outside (S1) the barrel field was studied to provide layer indices in order to determine whether the connections are of feedforward, feedback or lateral type. Single axons were reconstructed and the size of their swellings was stereologically sampled. The negative layer indices in S1 and S1BF and the layer index near zero in V1 indicate that the connection from S1BF to V1 is of feedback type while the opposite is of lateral type. The greater incidence of larger axonal swellings in the projection from V1 to S1BF strongly suggests that S1BF receives a stronger driver input from V1 and that S1BF inputs to V1 have a predominant modulatory influence.

Key words: corticocortical connections, cross-modal, feedback, feedforward, visuo-haptic interaction

Introduction

Multisensory integration is important for the formation of a coherent percept, to enhance the salience of biologically meaningful events and for the facilitation of adaptive behaviors (Stein and Meredith 1993; Ernst and Bulthoff 2004; Stein and Stanford 2008). Although it is clearly established that multisensory convergence occurs in higher order temporal, parietal and frontal cortices (Kaas and Collins 2013), numerous studies in primates, carnivores and rodents demonstrate that early sensory cortices are also involved in multisensory processing (Giard and Peronnet 1999; Foxe et al. 2000; Laurienti et al. 2002; Schroeder et al. 2003; Clavagnier et al. 2004; Brosch et al. 2005; Cappe and Barone 2005; Ghazanfar and Schroeder 2006; Macaluso 2006; Bizley et al. 2007; Driver and Noesselt 2008; Bizley and King 2009; Iurilli et al. 2012; Falchier et al. 2013; Sieben et al. 2013; Yoshitake et al. 2013; Hishida et al. 2014).

In contrast to primates (Falchier et al. 2002; Rockland and Ojima 2003; Clavagnier et al. 2004; Cappe and Barone 2005), there are significant direct connections between primary sensory cortices in rodents (Miller and Vogt 1984; Paperna and Malach 1991; Budinger et al. 2006; Wang and Burkhalter 2007; Budinger and Scheich 2009; Campi et al. 2010; Charbonneau et al. 2012; Iurilli et al. 2012; Sieben et al. 2013; Henschke et al. 2014; Stehberg et al. 2014; Zingg et al. 2014). The mouse is therefore an interesting model for the study of multisensory integration at the level of primary sensory cortices.

The hierarchical organization of cortical connectivity has been defined by feedforward and feedback pathways (Rockland and Pandya 1979; Felleman and Van Essen 1991). Although there are some differences in the morphological features of these connections, this classification also seems to apply to rodents (Godement et al. 1979; Coogan and Burkhalter 1990,

1993; Gonchar and Burkhalter 1999, 2003; Yamashita et al. 2003; Berezovskii et al. 2011). Although primary sensory cortices might be expected to be at the same basal level of the cortical hierarchy and linked by symmetrical reciprocal connections, this is not always the case. Retrograde tracing studies have shown that the primary auditory and somatosensory cortices project in a feedback manner to the primary visual cortex (Charbonneau et al. 2012; Henschke et al. 2014), the primary visual cortex projects in a feedforward manner to the primary auditory cortex and in a lateral manner to the primary somatosensory cortex, and the primary auditory and somatosensory cortices are linked by reciprocal feedback projections (Henschke et al. 2014). This suggests that primary sensory cortices might be at different levels of the cortical hierarchy. Moreover these projection patterns have not been corroborated by the laminar distribution of anterogradely labeled terminals.

There is evidence for two types of glutamatergic synaptic contacts in corticocortical connections (Covic and Sherman 2011; De Pasquale and Sherman 2011; Petrof and Sherman 2013). Class 1 synapses have larger initial excitatory postsynaptic potentials, exhibit paired-pulse depression, are limited to ionotropic glutamate receptor activation and are anatomically correlated with larger synaptic terminals. Class 2 synapses have smaller initial excitatory postsynaptic potentials, exhibit paired-pulse facilitation, are limited to metabotropic glutamate receptor activation and are anatomically correlated with smaller synaptic terminals (see Sherman and Guillery 2013a). Class 1 and 2 are respectively considered drivers and modulators (Sherman and Guillery 1996, 1998; Reichova and Sherman 2004; Lee and Sherman 2008, 2009a, 2009b; Viaene et al. 2011; Petrof and Sherman 2013). We might expect that direct connections between primary sensory cortices comprise mainly Class 2 synapses.

The reciprocal projections between the primary visual cortex and the somatosensory cortex in mouse will be studied in order to quantify the relative strengths of the connections with both retrograde and anterograde neuronal tracers. The size and laminar density of axonal swellings will be studied in order to see whether these direct projections between primary sensory cortices fit in the classification criteria provided by the distribution of retrogradely labeled neurons and if they present features of driving or modulatory corticocortical inputs.

Methods

Animals were treated in accordance with the regulations of the Canadian Council for the Protection of Animals and the study was approved by the Animal Care committee of the Université du Québec à Trois-Rivières. C57Bl/6J mice (n = 20) (Charles River, Montréal, QC, Canada) from our colonies were used. All animals were kept under a light/dark cycle of 14/10 h and were adults when sacrificed.

Tracing Procedures

Surgical anesthesia was achieved and maintained with inhalation of 1.5–2.5% isoflurane and vital signs were monitored throughout the procedures. The animals were mounted on a stereotaxic apparatus. Mice were protected from ocular dryness by applying ophthalmic ointment (Polysporin; Pfizer, Toronto, ON, Canada). A scalp incision was made along the midline to expose the skull. For injections in the primary visual cortex (V1), a small craniotomy was performed 3.7 mm caudal and 2.5 mm lateral to Bregma or, for injections in the barrel field of the primary somatosensory cortex (S1BF), 1.5 mm caudal to Bregma and 2.9 mm from the midline. The dura was incised and a glass micropipette filled with a solution of the b-fragment of cholera toxin (CTb) or biotinylated dextran amine (BDA) was inserted into the cortex. Retrograde and anterograde neuronal tracing was achieved with iontophoretic injections of 1% solution of CTb and of a 10% solution of high-molecular weight BDA (10 kDa) respectively in phosphate-buffered saline (PBS) (Molecular Probes, Cedarlane Laboratories, Ontario, Canada) through glass micropipettes (20 μm tip diameter) into V1 for 5 animals and S1BF for 5 animals for each tracer. A 1.5 μA positive current with a 7-s duty cycle was applied for 10 min, starting at a depth of 500 μm and ending at 100 μm from the pial surface, 2 min at each 100 μm. The mice were kept warm until they recovered from anesthesia and postoperative pain was managed with buprenorphine Temgesic, Schering-Plough, Hertfordshire, UK; (i.p.; 0.009 mg/kg) injected before anesthesia was induced.

After a 2-day survival period following CTb injections and a 7-day survival period following BDA injections, mice received an intraperitoneal injection of 120 mg/kg sodium pentobarbital (Euthanyl; Bimeda-MTC, Cambridge, ON, Canada) and were perfused through the heart with PBS (pH 7.4) followed by phosphate-buffered 4% paraformaldehyde. Brains were harvested, postfixed for 1–2 h, cryoprotected with 30% sucrose and frozen prior to sectioning and CTb or BDA processing.

Serial 50-μm-thick coronal sections were taken using a freezing microtome. One series was processed for CTb immunohistochemistry and the other was mounted on slides and stained with cresyl violet to identify the cortical areas and layers. Sections processed for BDA histochemistry were counterstained with bisbenzimide to identify the cortical areas and layers.

To visualize CTb-labeled neurons, free-floating sections were treated for 45 min with 0.15% H_2O_2 and 70% methanol to quench endogenous peroxidase and thoroughly rinsed in 0.05 M Tris-HCl-buffered 0.9% saline solution (TBS, pH 8.0) containing 0.5% Triton X-100 (TBSTx). Sections were then incubated in 2% normal donkey serum (NDS) for 2 h and transferred to a solution of primary antibody (goat polyclonal anti-CTb 1:20 000; Molecular Probes) with 1% NDS in PBS-Tx for 2 days at 4°C. Subsequently, sections were rinsed in PBS-Tx and incubated in a secondary antibody (biotinylated donkey anti-goat; 1:500; Molecular Probes) solution with 1% NDS in PBS-Tx for 2 h at room temperature. Following further rinsing, the sections were then incubated for 90 min in an avidin–biotin complex solution (Elite Vectastain, Vector Laboratories, PK4000 Standard kit) in TBS-Tx, pH 8.0, rinsed in TBS, and then incubated in a 0.015% 3'-diaminobenzidine (DBA) solution. Labeled neurons were revealed by the addition of 0.005% H_2O_2. Sections were washed and mounted on gelatin-subbed slides, air-dried, dehydrated and cover-slipped with Permount mounting media (Fisher Scientific, Ottawa, ON, Canada).

For BDA staining, after quenching endogenous peroxidase, sections were incubated for 90 min in an avidin–biotin complex solution (ABC Vectastain elite), washed and BDA was revealed using nickel-intensified DAB (Sigma-Aldrich, St. Louis, MO, USA) as a chromogen. Sections were pre-incubated for 30 min in Tris-buffered (TB) (0.05 m)-nickel ammonium sulfate 0.4%, pH 8.0, followed by 10 min in TB-nickel ammonium containing 0.015% DAB and 0.005% H_2O_2. Sections were dehydrated in ethanol, cleared in xylenes and cover-slipped with Eukitt mounting media.

Charting of Retrogradely Labeled Neurons

All CTb retrogradely labeled neurons on one of every two sections of S1, S1BF and of V1 were plotted using an Olympus

BX51WI microscope (×20, 0.75 NA objective) equipped with a three-axis computer-controlled stepping motor system coupled to a personal computer and to a color Optronix CCD camera and driven by the Neurolucida software (MBF Biosciences, Williston, VT, USA).

The whole primary somatosensory and visual cortices were systematically and randomly sampled on sections spaced 200 μm apart. Cortical areas were delineated at lower magnification (×4, 0.16 NA objective) on adjacent Nissl-stained sections. Borders between cortical areas were delineated according to the cytoarchitectonic descriptions provided by Caviness (1975) and the mouse brain atlas of Franklin and Paxinos (2008). Contours of each cortical area in which retrogradely labeled cells were located were traced with Neurolucida and the limits of each cortical layer were traced. These contours were superimposed on the images of CTb-reacted sections and resized for shrinkage differences between the Nissl and CTb sections. This allowed plotted neurons in each cortical area to be assigned to either supragranular, granular or infragranular layers for the calculation of layer indices. These indices provide a quantitative assessment of the laminar distribution of retrogradely labeled neurons and are instrumental in the classification of corticocortical feedback, feedforward and lateral connections (Felleman and Van Essen 1991). Layer indices (*L*) were calculated using the formula:

$$L = (S - I)/(S + I)$$

where *S* and *I* are the numbers of labeled neurons in supragranular and infragranular layers respectively (Budinger et al. 2006, 2008; Budinger and Scheich 2009). The indices range between –1 and 1. Negative values indicate feedback connections mostly originating in infragranular layers and positive values indicate feedforward connections mostly originating in supragranular layers. Values near zero indicate lateral connections. All photomicrographs were cropped, and luminosity and contrast were adjusted with Adobe Photoshop software.

Single Axon Reconstructions

Six anterogradely labeled axons projecting from V1 to the barrel field of S1 and six axons projecting from the barrel field of S1 to V1 were reconstructed at higher magnification (×100, 1.4 NA objective). Cortical areas were delineated at lower magnification (×4, 0.16 NA objective) using bisbenzimide as a fluorescent counterstain. Contours of each cortical area in which anterogradely labeled axons were located were traced with Neurolucida and the limits of each cortical layer were defined. Axons were reconstructed from their entrance in the gray matter. The axonal branches were completely reconstructed and followed throughout the serial sections until they ended and could not be followed further to adjacent sections. Throughout the full extent of the axonal arborization, all the axonal swellings were charted, assigned to specific cortical layers and their largest diameter was measured. The size frequency distribution of axonal swellings was determined for each cortical layer of each individual axon.

Stereological Sampling of Laminar Distribution of Axonal Swellings

In order to provide an unbiased size frequency distribution of swellings in each cortical layer for the projection from V1 to the S1 barrel field and the reciprocal projection from the S1 barrel field to V1, a stereological systematic random sampling of these projection fields was performed using the Stereo Investigator software (MBF Bioscience) in cases that received a columnar injection in the visual or somatosensory cortices. These size distributions for a whole population of neurons projecting from the injection sites were compared with the same distributions obtained for individual axons and with the sum of all the single axon reconstructions. This comparison is done to assess if the data obtained from the swellings of single axons is representative of the whole population of swellings sampled.

Projections fields in which anterograde labeling was observed were sampled using the optical fractionator workflow (in Stereo Investigator) on approximately 10 equidistant sections covering the full anteroposterior range of the projection, except for the fourth case injected with BDA in V1 in which the projection extended to only 5 sections. On each section, polygonal contours were traced around the projection field in each cortical layer. Axonal swellings were then counted in no less than 100 disectors that were $20 \times 20\ \mu m^2$ square and 15 μm height, and evenly distributed at the intersections of a $80 \times 80\ \mu m^2$ grid. The maximum diameter was measured for each sampled swelling.

This optical fractionator sampling strategy allowed for the estimation of the total number of swellings in each cortical layer. The total numbers of swellings (*N*) were calculated by the following equation (West et al. 1991):

$$N = \sum Q \times ssf^{-1} \times asf^{-1} \times tsf^{-1}$$

where ΣQ is the total number of swellings counted within the disectors, ssf is the section sampling fraction (number of sampled sections over the total number of sections on which the terminal projection field appears), asf is the area sampling fraction (ratio of the frame area/the total area of the reference space on the section) and tsf is the thickness-sampling fraction (disector height/section thickness). Product of ssf, asf and tsf is the overall sampling faction (see Table 1). Coefficients of error (CEs) were calculated according to the procedure described by West and Gundersen (1990), in order to determine whether the sampling effort was sufficient. It is widely accepted as a rule of thumb that CEs below 0.1 are indicative of a sufficient sampling. The objective of this stereological sampling was not to determine the total number of swellings that are labeled for each injection. This number is a function of the injection size. The objective was to obtain unbiased estimates of laminar and size distributions.

Sampling of Axonal Diameters

In order to compare the caliber of the axonal population entering the cortical areas V1 and the somatosensory barrel field, the initial diameter of the axons as they leave the white matter to enter the cortical gray layers was calculated. Axonal diameter changes over short distances and a single point measurement of the axonal diameter was not deemed adequate. To take this into account and to obtain an unbiased estimate of the axons diameters, a weighted average of diameter for the initial 25 μm of each axon was calculated. These diameters are not the caliber of the axons as they emerge from the neuronal cell bodies but rather the caliber of the axons distally, as they enter their target, which is either S1BF or V1.

The Neurolucida software encodes axons as a succession of small segments. Each segment is attributed coordinates in three-dimensional space, a length and a diameter. These

Table 1 Stereological sampling parameters for the estimation of the number of anterogradely labeled axonal swellings in each layers in S1BF after injections of BDA into V1 of C57Bl/6 mice

Case	Layer	Number of sections	Total area (mm^2)	Number of disectors	Number of objects	Sampling fraction	Total estimation	CE
1	I–III	9	8661	106	313	0.004	84 662	0.060
	IV	9	5663	117	164	0.006	26 279	0.053
	Va	9	3150	117	178	0.011	15 865	0.065
	Vbc	9	5407	115	164	0.006	25 527	0.050
	VI	9	3950	116	78	0.009	8793	0.097
	Total (Mean)	45	26 831	571	897	(0.007)	161 126	(0.065)
2	I–III	9	6593	112	329	0.005	64112	0.074
	IV	9	4580	111	118	0.007	16117	0.075
	Va	9	2257	128	139	0.017	8115	0.074
	Vbc	9	3969	119	129	0.009	14243	0.089
	VI	9	2050	111	80	0.016	4890	0.083
	Total (Mean)	45	19 449	581	795	(0.011)	107477	(0.079)
3	I–III	9	17 372	110	317	0.002	165717	0.075
	IV	9	11 941	112	158	0.003	55764	0.052
	Va	9	6617	127	181	0.006	31218	0.060
	Vbc	9	10 180	123	156	0.004	42 739	0.051
	VI	9	10 885	64	111	0.003	20 776	0.063
	Total (Mean)	45	56 995	536	923	(0.004)	316 214	(0.060)
4	I–III	5	2507	106	174	0.013	13 519	0.194
	IV	5	1521	105	72	0.021	3427	0.201
	Va	5	940	114	60	0.037	1626	0.192
	Vbc	5	1408	110	90	0.024	3786	0.147
	VI	5	1515	105	141	0.021	6685	0.167
	Total (Mean)	25	7891	540	537	(0.023)	29 043	(0.180)
5	I–III	10	5745	118	97	0.006	17 793	0.071
	IV	10	3005	105	38	0.009	4097	0.097
	Va	10	1821	120	63	0.018	3602	0.044
	Vbc	10	2506	115	42	0.012	3449	0.052
	VI	10	1398	112	40	0.021	1881	0.070
	Total (Mean)	50	14 475	570	280	(0.013)	30 822	(0.067)

segments correspond to the interval between two mouse clicks as the observer traces the axons. These clicks will be done to record changes in direction and/or diameter of the axons. The data were used to calculate the average diameter over the first 25 μm of the tracing from the point of entry of the axons into the cortical gray matter, weighted by the length of the segments recorded over this distance.

The sampling of the measured axons was performed on the same sections that were used for the stereological sampling of axonal swellings (see Tables 1 and 4) to insure that axons were systematically and randomly selected. Axons were selected as they crossed the line between the white and gray matter. The total length of this line for each case and the number of sampled sections are given in Table 2.

Table 2 Sampling parameters for the estimation of the diameter of anterogradely labeled axons as they enter the gray matter in S1BF and V1 after injections of BDA into V1 and S1BF respectively of C57-Bl/6 mice

Injection site	Case	Number of sections	Sampled length (mm)	Number of axons
V1	1	9	13.281	259
	2	9	12.215	116
	3	9	14.372	104
	4	5	6.567	195
	5	10	13.967	132
S1BF	1	11	11.532	134
	2	10	6.016	38
	3	10	5.373	154
	4	7	6.215	84
	5	8	6.143	310

Statistical Analysis

Statistical analyses were performed using SPSS v 16.0 software (SPSS, Chicago, IL, USA).

Results

Labeling of Cortical Visuotactile Connections with CTb

Representative CTb injection sites in the visual cortex are illustrated in Figure 1A (V1) and in the somatosensory barrel field in Figure 1B (S1BF). None of the injections damaged the underlying white matter. In all cases, CTb injections in S1BF and V1 anterogradely labeled axonal terminals and retrogradely labeled numerous neuronal cell bodies in V1 and S1 respectively. Conversely, CTb injections outside of the barrel field of S1 resulted in very few labeled neurons in V1.

In S1, CTb-labeled neurons were found in supragranular layers and layer 4 but they were more numerous in infragranular layers (Fig. 1C). By contrast, in V1, CTb-labeled neurons were more evenly distributed in layers 2/3 to layer 5 (Fig. 1D). In layer 6,

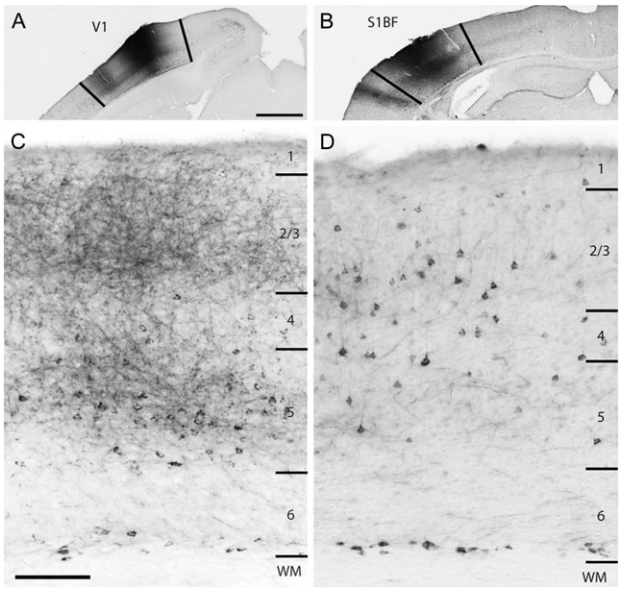

Figure 1. *A*: An injection of CTb in V1 produced in *C*: Anterograde and retrograde labeling in S1BF. Note the more abundant retrogradely labeled neurons in layer 5 than in supragranular layers and the intense anterograde labeling in layers 2/3 and 5. *B*: An injection of CTb in S1BF produced in *D*: Retrogradely labeled neurons in supragranular and infragranular layers, a typical distribution of lateral connections. Scale: 1000 μm (*A*/*B*) and 200 μm (C/D).

neurons with fusiform cell bodies were found along the border of the white matter.

In addition, CTb injections in V1 produced intense anterograde axonal labeling in supragranular layers as well as in layer 5. Less intense axonal labeling was observed in layer 4 and only sparse labeling was observed in layer 6 (Fig. 1C). Injections in S1BF produced sparse anterograde labeling in all layers of V1, (Fig. 1D). Anterograde labeling was much lighter in the projection from S1BF to V1 than that of V1 to S1BF. This clearly shows an asymmetry of the reciprocal connections between V1 and S1BF; the projection from V1 to the S1BF being much stronger.

Even though the number of labeled neurons varied between cases, and is dependent upon the injection size, all injections were performed with the same parameters and a comparison of the total number of labeled neurons is instructive here of the strength of the projection. Following CTb injections in V1, the number of retrogradely labeled neurons in S1BF ranged between 10 and 164 (mean = 80.8) and between 15 and 85 (mean = 36.6) in S1 (Table 3), but this difference was not significant (one-way ANOVA, $p = 0.857$) (Fig. 2A).

Similarly, injections of CTb in and outside the somatosensory barrel field retrogradely labeled neurons in V1. Very few neurons were labeled after injections in S1. Of the 5 cases injected with CTb in S1, 3 of them had no retrogradely labeled neurons in V1 and 2 of them had only 2 neurons labeled in layer 5 of V1. Conversely, numerous neurons were labeled in V1 following injections in S1BF. The total number of labeled neurons in V1 following S1BF injections ranged between 163 and 679 (mean 446) (Table 3). There was a statistically significant difference between the projections (Kruskal–Wallis, $p = 0.001$) Post-hoc tests revealed that the projection from V1 to S1BF was stronger than that from S1 to V1 (Tukey-HSD, $p = 0.001$) and from S1BF to V1 (Tukey-HSD, $p = 0.002$) (Fig. 2A). This is in agreement with the stronger projection of V1 to the S1BF shown by CTb anterograde labeling.

Laminar Distribution of Cholera Toxin b Labeled Neurons

In order to classify each projection as a feedforward, feedback or lateral connection, retrogradely labeled neurons in V1 and in the somatosensory cortex within and outside of the barrel field were counted in supragranular layers 1–3, layer 4 and infragranular layers 5 and 6 in each case (Table 3). Injections in V1 retrogradely labeled a greater percentage of neurons in infragranular layers 5 and 6 in S1 and S1BF (67.76% in S1 and 76.73% in S1BF), whereas injections in S1BF retrogradely labeled a greater percentage of neurons in the supragranular layers 1–3 (37.71%), (Fig. 2B). More specifically, following injections in V1, the percentage of labeled neurons in S1 was significantly lower in layer 4 (10.93%) than in layers 1–3 (23.93%) ($p = 0.016$), 5 (37.16%) ($p < 0.001$) and 6 (30.60%) ($p = 0.001$). There was no significant difference between the percentage of labeled neurons in layer 5 (37.16%) and 6 (30.60%) ($p = 0.848$). The percentage of labeled neurons in S1BF was significantly lower in layers 1–3 (15.59%) and layer 4 (7.67%) than in layer 5 (37.87%) ($p < 0.001$) and 6 (38.86%) ($p < 0.001$). There was no significant difference between the percentage of labeled neurons in layer 5 (37.87%) and in layer 6 (38.86%) ($p > 0.999$). Injections in S1BF resulted in a significantly greater percentage of labeled neurons in layers 1 to 3 (37.71%) in V1 than in layer 4 (21.61%) ($p = 0.029$), 5 (21.88%) ($p = 0.046$) and 6 (18.79%) ($p = 0.004$). There was no significant difference between the percentage of labeled neurons in layer 5 (21.88%) and in layer 6 (18.79%) ($p > 0.999$). Note that the proportion of neurons labeled in layers 5 and 6 were always similar showing that these layers do not vary independently.

Significant differences in the percentage of labeled neurons in cortical layers were observed between the projection from V1 to S1BF and S1BF to V1 (Fig. 2B). A greater proportion of labeled neurons was found in layers 1 to 3 of V1 following injections in S1BF compared with S1BF ($p < 0.001$) following injections in V1. A greater proportion of labeled neurons was found in layer 4 of V1 following injections in S1BF compared with S1 ($p = 0.033$) and S1BF ($p = 0.006$) following injections in V1. A lesser proportion of labeled neurons was found in layer 5 of V1 following injections in S1BF compared with S1 ($p = 0.019$) and S1BF ($p = 0.016$) following injections in V1. Also, a greater proportion of labeled neurons was found in layer 6 of S1BF following injections in V1 compared with S1 ($p = 0.036$) following injections in V1 and V1 ($p < 0.001$) following injections in S1BF.

Following CTb injections in V1, there were more labeled neurons in infragranular than in supragranular layers of S1 and S1BF. Hence, layer indices were negative in all cases ranging between −0.62 and −0.19 in S1 and between −1.0 and −0.54 in S1BF (Table 3), clearly suggestive of a feedback projection. CTb injections in S1BF produced retrograde labeling of neurons in similar proportion in supra- and infragranular layers in V1 and, in all cases, layer indices were near zero, ranging from −0.19 to 0.15 (Table 3) indicating a lateral type of connection between two areas of similar hierarchical levels within the cortical network. There was a statistically significant difference between the layer indices (Kruskal–Wallis, $p = 0.003$). Post-hoc tests reveal that the layer indices of V1 and both S1 and S1BF (Tukey-HSD, $p = 0.003$ and $p < 0.001$ resp) (Fig. 2C) were significantly different.

Anterograde BDA Labeling of Visuotactile Connections

The injections of high-molecular weight BDA in both V1 and S1BF resulted in significant anterograde axonal labeling in S1BF

Table 3 Numbers and percentage (in parentheses) of retrogradely labeled neurons in cortical layers and layer indices in S1, S1BF and V1 after injections of CTb into V1 and S1BF of C57Bl/6 mice

Injection site	Case	Layer	S1	S1BF	V1
V1	CT9	I–III	14 (16.47)	23 (14.02)	–
		IV	11 (12.94)	25 (15.24)	–
		V	33 (38.82)	55 (33.54)	–
		VI	27 (31.77)	61 (37.20)	–
		Layer Index	−0.62	−0.67	–
	CT20	I–III	4 (25)	0 (0)	–
		IV	0 (0)	0 (0)	–
		V	9 (56.25)	3 (30)	–
		VI	3 (18.75)	7 (70)	–
		Layer Index	−0.5	−1	–
	CT25	I–III	4 (26.67)	13 (23.21)	–
		IV	0 (0)	0 (0)	–
		V	5 (33.33)	27 (48.21)	–
		VI	6 (40)	16 (28.57)	–
		Layer Index	−0.47	−0.54	–
	CT26	I–III	6 (15.39)	19 (16.96)	–
		IV	8 (20.51)	6 (5.36)	–
		V	13 (33.33)	41 (36.61)	–
		VI	12 (30.77)	46 (41.07)	–
		Layer Index	−0.61	−0.64	–
	CT31	I–III	11 (39.29)	8 (12.9)	–
		IV	1 (3.57)	0 (0)	–
		V	8 (28.57)	27 (43.55)	–
		VI	8 (28.57)−0.19	27 (43.55)	–
		Layer Index		−0.74	–
S1BF	03-02b4	I–III	–	–	89 (31.79)
		IV	–	–	60 (21.43)
		V	–	–	84 (30)
		VI	–	–	47 (16.79)
		Layer Index	–	–	−0.19
	04-01b2	I–III	–	–	175 (34.38)
		IV	–	–	104 (20.43)
		V	–	–	86 (16.90)
		VI	–	–	144 (28.29)
		Layer Index	–	–	−0.14
	03-02b5	I–III	–	–	282 (47.08)
		IV	–	–	110 (18.36)
		V	–	–	108 (18.03)
		VI	–	–	99 (16.53)
		Layer Index	–	–	0.15
	03-02b6	I–III	–	–	68 (41.72)
		IV	–	–	38 (23.31)
		V	–	–	37 (22.70)
		VI	–	–	20 (12.27)
		Layer Index	–	–	0.08
	03-02b7	I–III	–	–	227 (33.43)
		IV	–	–	170 (25.04)
		V	–	–	173 (25.48)
		VI	–	–	109 (16.05)
		Layer Index	–	–	−0.11
	Mean ± SEM	I–III	7.8 ± 2.25 (23.93)	12.6 ± 4.54 (15.59)	168.2 ± 45.25 (37.71)
		IV	4 ± 2.57 (10.93)	6.2 ± 5.41 (7.67)	96.4 ± 25.49 (21.61)
		V		30.6 ± 9.65 (37.87)	
		VI	13.6 ± 5.61 (37.16)	31.4 ± 11.02 (38.86)	97.6 ± 24.73 (21.88)
		Layer Index	11.2 ± 4.71 (30.60)	−0.66 ± 0.09	
			−0.52 ± 0.09		83.8 ± 24.89 (18.79)
					−0.04 ± 0.08

and V1 respectively, without significant signs of retrograde transport. None of the injections damaged the underlying white matter. The BDA injections in the barrel field of S1 (Fig. 3A) resulted in anterogradely labeled axons in V1 in each of the 5 cases, confirming the projection observed following the injection of CTb in V1. These injections labeled axons in infra-

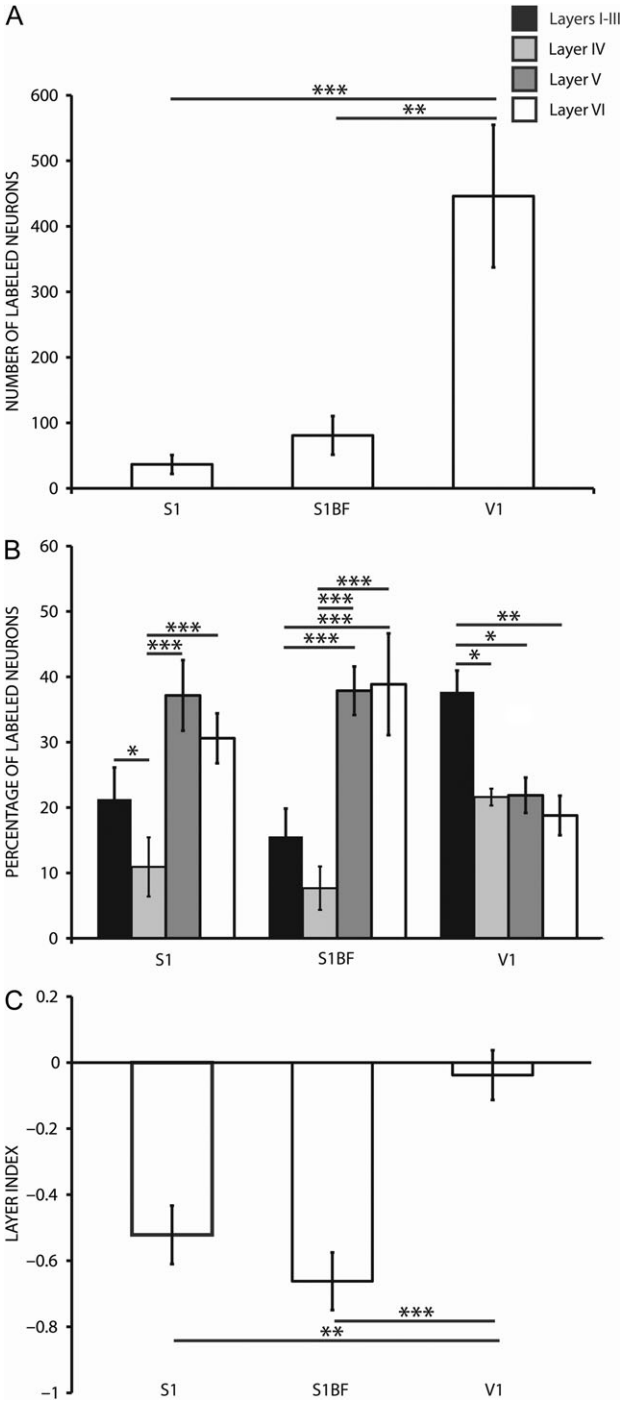

Figure 2. A: Number of retrogradely labeled neurons in cortical areas following an injection of CTb in V1 and S1BF of C57Bl/6 mice. B: Percentage of retrogradely labeled neurons in cortical areas following an injection of CTb in V1 and S1BF of C57Bl/6 mice. C: Layer indices for neocortical areas following an injection of CTb in V1 and S1BF of C57Bl/6 mice.

and supragranular layers of V1 (Fig. 3B). Upon entering the gray matter, axons traveled up to layer 4 without extensive branching. Some small *en-passant* axonal swellings were seen as the axons crossed layer 4. In supragranular layers a dense lattice of intercrossing neurites was always present. Labeled terminals were most evident in layers 1–3, with a greater density in the superior part of layer 2.

Injections in V1 (Fig. 3C) anterogradely labeled axonal arbors largely restricted to the barrel field in S1, in each of the 5 cases, confirming the projection observed following the injection of CTb in S1BF. Labeled axons were found in infra- and supragranular layers of (Fig. 3D). Axons left the white matter, crossed layer 6 and arborized in layer 5. Axons traveled radially through the granular layer without significant branching. Axonal terminal labeling was most intense in the supragranular layers.

Single Axon Branching Morphology

In order to characterize the branching structure and the laminar and size distribution of axonal swellings, a sample of single axons were completely reconstructed from their entrance in the gray matter for the projections from V1 to S1BF and from S1BF to V1. More specifically, branching structure was described in terms of the general appearance of the axons and axonal swellings were described with respect to their laminar position and size distribution.

Axons of the projection from V1 to S1BF (Fig. 4) displayed a wide range of branching structures. Relatively simple branching patterns were observed in three axons (Fig. 4A, C and F). Upon entering the gray matter, these axons ascended through the infragranular layers without any significant branching, and underwent a few bifurcations within the supragranular layers, forming relatively restricted columnar trees. One axon branched mostly in the supragranular layers but sparsely in infragranular layers and exhibited a somewhat more complex richly arborized tree (Fig. 4D). The medio-lateral extent of the portion of the arbor located in the supragranular layers was wider in this axon than in the more simple ones which had a more restricted projection column. In these three axons, axonal swellings were mostly located in supragranular layers, reflecting their branching structure.

Two axons had more extensive trajectories in the infragranular layers than the other axons of the sample (Fig. 4B and E). One axon (Fig. 4B) bifurcated early after entering the gray matter, sending a long poorly branched extension that coursed tangentially over more than 500 μm in layers 5 and 6, and another branch that ascended through layers 5 and 4 that subsequently arborized sparsely in supragranular layers forming a very restricted radial projections in layers 1–3. Finally, one axon exhibited extensive tangential travel in the infragranular layers (Fig. 4E). As in the previously described axon, it bifurcated only once to produce two main branches. One ascended to the supragranular layers and formed a tangentially restricted projection column, whereas the other bifurcated in layer 5 in one location (see terminal branches 1 and 3) and another branch traveled extensively over more than 500 μm to ascend in the supragranular layers without any significant branching in another location in the barrel field. In these two axons, (Fig. 4B and E) swellings were quite evenly distributed across all cortical layers also reflecting to distribution of axonal segments in these cases.

The size distribution of swellings on individual axons in the projections from V1 to S1BF shows a great predominance of very small swellings (Fig. 4) with a small contingent of much larger swellings. In four of the six reconstructed axons, the largest swellings were no larger than 1.9 μm in diameter (Fig. 4A–D). On two axons, there were some swellings with diameters greater than 2.5 μm (Fig. 4E and F, 2.8 and 2.7 μm resp.).

Axons in the projection from S1BF to V1 (Fig. 5) also displayed diverse morphologies. Three axons showed an extensive tangential coverage (Fig. 5A, B and F). In the axon depicted in

Table 4 Stereological sampling parameters for the estimation of the number of anterogradely labeled axonal swellings in each layers in V1 after injections of BDA into S1BF of C57Bl/6 mice

Case	Layer	Number of sections	Total area (mm^2)	Number of disectors	Number of objects	Sampling fraction	Total estimation	CE
1	I–III	11	9174	124	201	0.004	53 794	0.089
	IV	11	6717	122	80	0.005	15 935	0.078
	Va	11	3229	141	85	0.012	7043	0.098
	Vbc	11	5130	137	137	0.007	18 558	0.085
	VI	11	6571	118	194	0.005	39 083	0.090
	Total (Mean)	55	30 821	642	697	(0.007)	134 413	(0.088)
2	I–III	10	1604	105	488	0.018	27 043	0.043
	IV	10	779	122	291	0.043	6747	0.056
	Va	10	461	129	241	0.077	3129	0.059
	Vbc	10	600	120	169	0.055	3070	0.072
	VI	10	566	118	89	0.058	1549	0.082
	Total (Mean)	50	4010	594	1278	(0.050)	41 538	(0.062)
3	I–III	10	1380	108	209	0.022	9692	0.061
	IV	10	578	119	153	0.057	2696	0.050
	Va	10	461	124	146	0.074	1971	0.061
	Vbc	10	649	128	128	0.054	2355	0.057
	VI	10	607	153	91	0.070	1310	0.059
	Total (Mean)	50	3675	632	727	(0.055)	18 024	(0.058)
4	I–III	7	3414	111	254	0.010	25 597	0.080
	IV	7	1343	133	106	0.030	3508	0.092
	Va	7	819	115	90	0.043	2102	0.099
	Vbc	7	1317	105	65	0.024	2671	0.094
	VI	7	1295	124	64	0.029	2190	0.093
	Total (Mean)	35	8188	588	579	(0.027)	36 068	(0.092)
5	I–III	8	1493	121	152	0.025	6192	0.052
	IV	8	709	139	82	0.059	1381	0.040
	Va	8	403	158	56	0.119	472	0.068
	Vbc	8	710	138	52	0.059	883	0.069
	VI	8	678	134	50	0.060	835	0.026
	Total (Mean)	40	3993	690	392	(0.064)	9763	(0.051)

Fig. 5A, the main trunk ascended through the infragranular layers without any branching. It gave off one collateral that circled in a small zone of the mid-supragranular layers before sending a descending unbranched extension back into the deep infragranular layers. The other branch ascended to layer 1 where it bifurcated in two branches (1 and 3 in Fig. 5A), one of which traveled without branching in layer 1 for a distance exceeding 400 μm.

Another axon showed an extensive tangential trajectory (Fig. 5B). Upon entering the gray matter, this axon made two successive right angle turns before ascending through the infragranular layers without branching. While in layer 5, it gave out one branch that ascended through infragranular layers without any significant branching, except for a small terminal tuft. The other branch emerged from layer 5 and traveled vertically in the deeper part of layer 5 and emitted therein several short collaterals and then engaged in a linear tangential course without branching for more than 300 μm. It subsequently made a sharp turn and ascended obliquely towards the pial surface in an anteriorly directed trajectory for approximately 400 μm but did not reach layer 1. The laminar distribution of swellings was similar in axons shown in Fig. 5A and B in that the majority were found in supragranular layers.

The axon depicted in Fig. 5F is peculiar in that it had a collateral branch that arborized quite significantly in layer 6 and another that ascended to the upper–half of the supragranular layers before arborizing. Also, the top-view of this axon showed that the infragranular focus of arborisation was out of radial register with the supragranular terminal arbors which were located about 300 μm more anteriorly. This is not apparent in the coronal projection that would rather suggest a more restricted columnar organization for this axon (Fig. 5F). The laminar distribution of swellings for this axon was clearly bimodal with an important population of swellings in supragranular layers and an also very important contingent of swellings in layer 6.

Two axons displayed a restricted tangential extent of their arborisation (Fig. 5C and D). They arborized more importantly in the supragranular layers even though they did emit a few unbranched collaterals in infragranular layers. Top projections of these axons demonstrated the restricted tangential distribution of their arbors that remained within a radius of approximately 300 μm. The tangential extent of the axons projecting from V1 to S1BF was in general greater than that of these two axons. The laminar distribution of swellings of the axon shown in Fig. 5C was similar to that of the axon of Fig. 5B, in that there

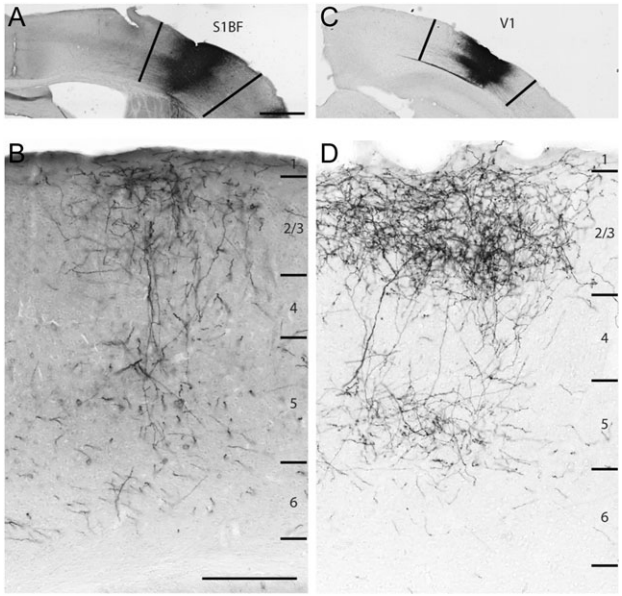

Figure 3. A: An injection of BDA in S1BF produced in B: Anterograde labeling of axons in the supragranular and infragranular layers in V1. C: An injection of BDA in V1 produced in D: Anterograde labeling of axons in the supragranular and infragranular layers in S1BF. Scale: 1000 μm (A/C) and 250 μm (B/D).

was a large contingent of swellings in supragranular layers, but also a significant number of swellings distributed throughout cortical layers. The axon depicted in Fig. 5E was peculiar in that it did not reach supragranular layers. Oblique segments ascended through the infragranular layers without any significant branching. Consequently, swellings were found in similar proportions only in layers 5 and 6.

The size distribution of swellings on individual axons in the projection from S1BF to V1 shows a strong dominance of very small swellings with diameters no greater than 1.2 μm (Fig. 5A, B, D–F). In all the six reconstructed axons, only one axon has a few swellings no larger than 1.8 μm in diameter (Fig. 5C).

Axonal Thickness

In order to compare the reciprocal projections between V1 to S1BF at the single axon level, the frequency distributions of the diameters of randomly sampled axons (Table 2) as they enter the gray matter were compared (Fig. 6). Within the sampled axons, the size of the mean diameters ranged between 0.1 and 1.9 μm for the projection from V1 to S1BF and between 0.1 and 0.5 μm for the projection from S1BF to V1. There was a very highly significant difference between the projection from V1 to S1BF and from S1BF to V1 (Kolmogorov–Smirnov tests, $p < 0.001$). In both projections, thin axons are predominant and account for the majority of the axons. In the projection from V1 to the somatosensory barrel field, quite thick axons were found that were never seen in the reciprocal projection from the barrel field to the visual cortex.

Number of Anterogradely Labeled Axonal Swellings

The total number of anterogradely labeled axonal swellings for each injection was estimated through stereological sampling in order to compare the strength of the reciprocal projections between the visual cortex and the somatosensory barrel field. The estimated numbers of anterogradely labeled axonal swellings in each layers of S1BF are shown in Table 1 and the numbers of anterogradely labeled axonal swellings in each layers of V1 are shown in Table 4.

Even though the total number of labeled swellings and axons is dependent upon the injection size, all our injections were performed with the same parameters and could, within certain limits, be compared. The estimated total number of swellings in S1BF following a BDA injection in V1 ranged between 29 043 and 316 214 (Table 1) with a mean of 128 936 and the estimated number of swellings in V1 after a BDA injection in S1BF ranged from 9763 to 134 413 (Table 4) with a mean of 47 961. This difference did not reach statistical significance (Mann–Whitney, $p = 0.251$).

Laminar Distribution of Axonal Swellings

The laminar and size distributions of axonal swellings in the sample of reconstructed single axons in V1 and S1BF (Fig. 7A and C) were compared with the stereological estimates of the laminar and size distributions of swellings labeled following large columnar injections of BDA in these cortices (Fig. 7B and D). The stereologically estimated numbers of anterogradely labeled axonal swellings in each layers of S1BF are shown in Table 1 and the numbers of anterogradely labeled axonal swellings in each layers of V1 are shown in Table 4.

Although the laminar distribution of swellings in individual axons exhibits a wide range of patterns (see Fig. 4 and 5), the sum of the reconstructed axons in S1BF and V1 produced similar laminar distributions of axonal swellings (Fig 7A). Furthermore, these distributions were very similar to those obtained with the stereological sampling of cortical layers (Fig. 7B). The stereological sampling produced smaller variances of the estimates of the number of axonal swellings (Fig. 7B). There were no significant differences in the estimated percentage of axonal swellings in each layer between V1 and S1BF (Kruskal–Wallis, $p = 0.946$).

In both the stereological sampling and the reconstructed axons, both injections in V1 and S1BF resulted in labeling of axons with swellings in layers 1–3 and 5. The proportion of swellings found in layer 4 was commensurate with those in infragranular sublayers 5a and 5c and also layer 6.

Size Distribution of Axonal Swellings in Cortical Layers

Within the stereological sample of axonal swellings, the size of the axonal swellings ranged between 0.3 μm and 2 μm for the projection from V1 to S1BF and between 0.3 μm and 0.9 μm for the projection from S1BF to V1. Within the sample of reconstructed axons, the size of the axonal swellings ranged between 0.3 μm and 2.8 μm for the projection from V1 to S1BF and between 0.2 μm and 1.8 μm for the projection from S1BF to V1.

The systematic random stereological sampling yielded size distributions of the swellings that should be representative of the population of swellings in these projections. The sample of reconstructed axons is quite small and is not statistically representative of the whole population. However, the stereological sampling scheme did not pick up the larger swellings that were observed in the reconstructed axons. These are quite rare in the overall population and could have been missed. Nevertheless the predominance of smaller swelling in all layers of the projection from S1BF to V1 was observed in both samples (Fig. 7C,D).

The laminar size distribution of axonal swellings was compared between the projection from V1 to S1BF and from S1BF to V1 in the samples of reconstructed axons (Fig. 7C) and the

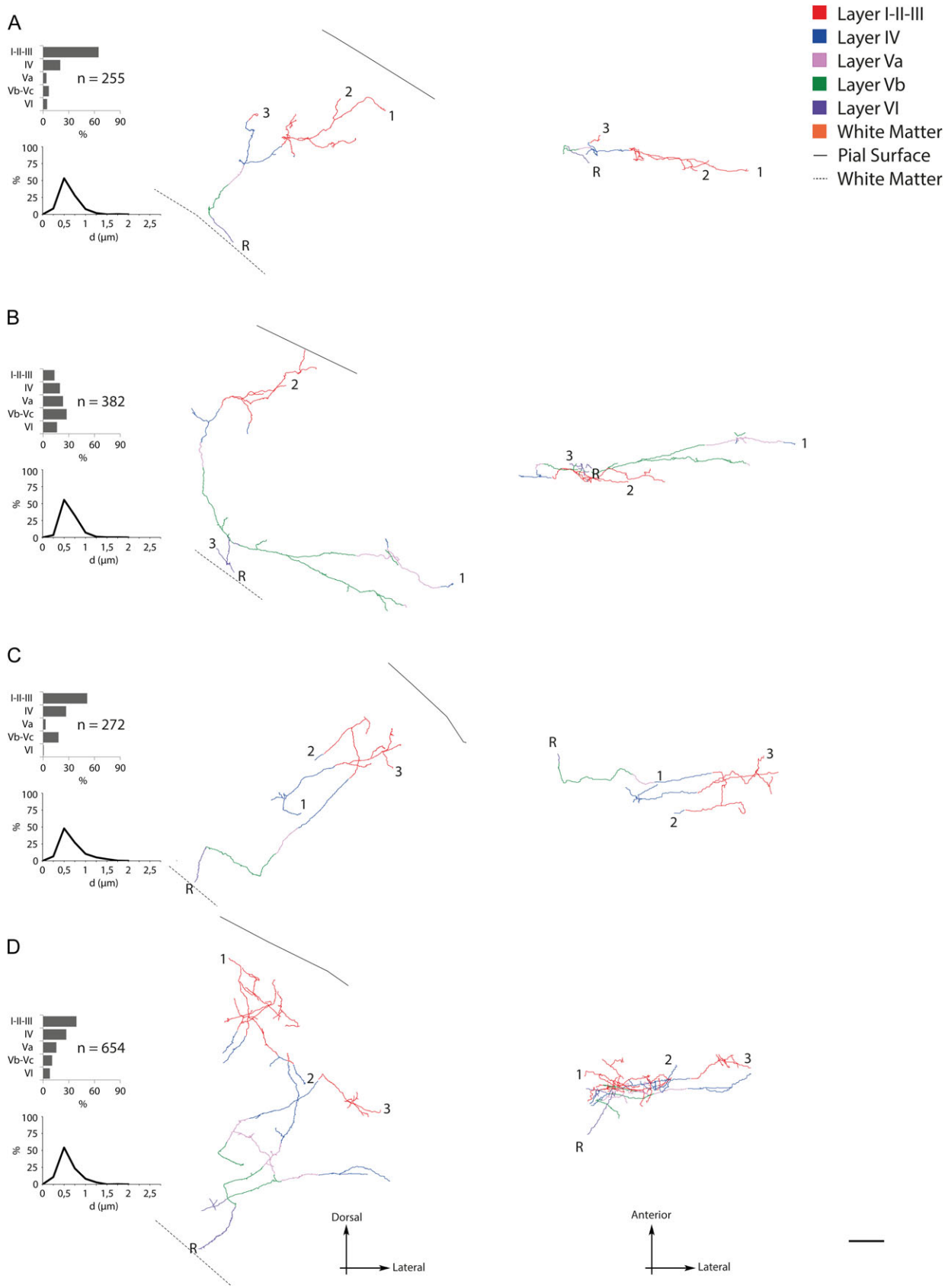

Figure 4. Single axons in S1BF following an injection of BDA in V1 of C57Bl/6 J mice. The reconstructed axons are viewed as coronal plane projections on the left panel and as top projections on the right. Each colored segment on the axons corresponds to the layer in which this segment is situated. The full line represents the pial surface and the dotted line the border between layer 6 and the white matter. The R is the root of the axons as they enter they gray matter. The numbers (1/2/3) on the axons are landmarks to facilitate the visualization of their structure in the two different projections. On the left of axonal structures are histograms of the laminar distribution of terminals (% of axonal swellings for each layer) *n* is the total number of axonal swellings for each axon; and just below is the size distribution of axonal swellings as a function of their largest diameter (*d*). Scale: 100 µm.

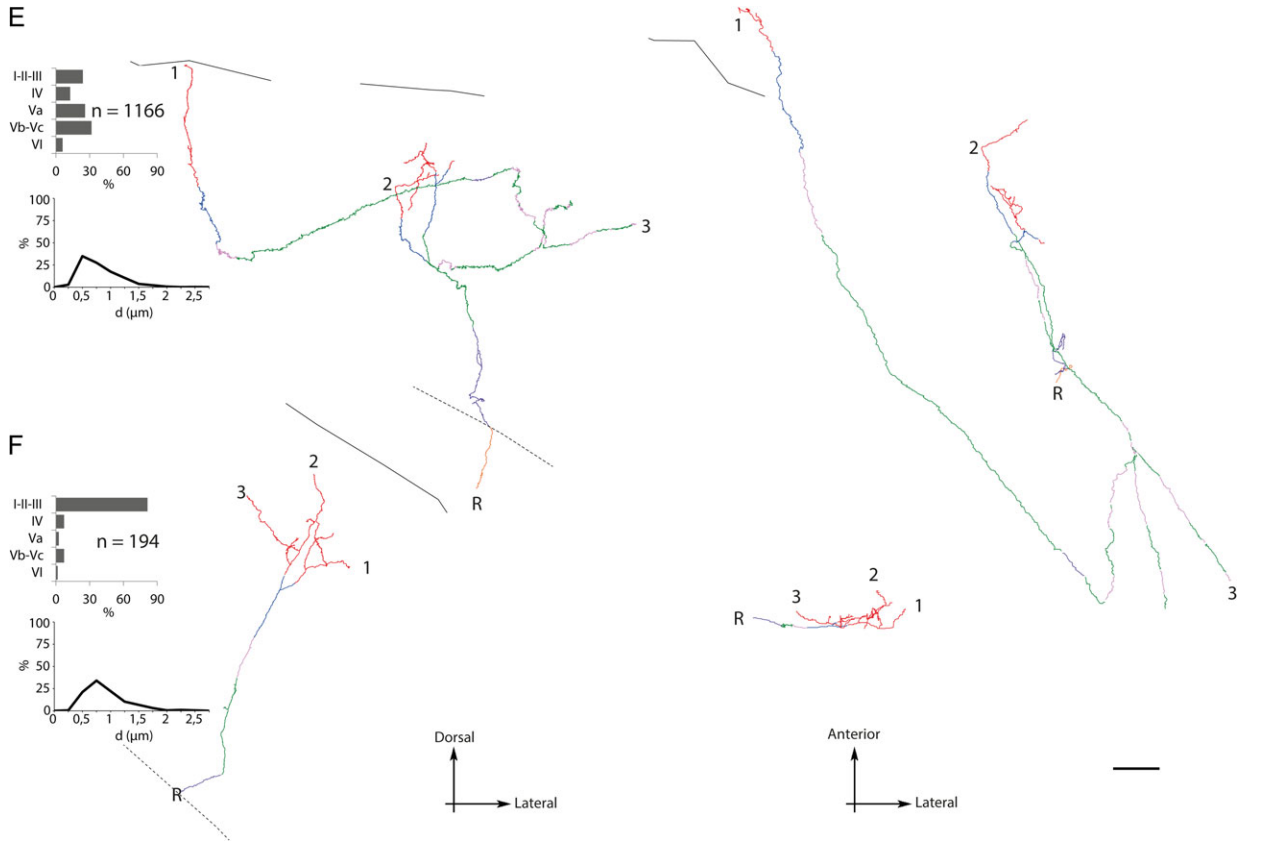

Figure 4. *Continued.*

stereological samples described above (Fig. 7D). The small sample of reconstructed axons is likely not sufficient to detect with any statistical power the swelling size differences between layers; only the statistical conclusions drawn from the stereological sampling will be considered here.

Within the projection from V1 to S1BF, there was a significant difference of the mean size of axonal swellings between layers (one-way ANOVA, p = 0.001), layer 6 swellings being smaller than those of layers 1 to 3 ($p = 0.001$) and layer 5a ($p = 0.001$) (Fig. 7D). Within the projection from S1BF to V1, the mean size of the axonal swellings was significantly different between layers (one-way ANOVA, $p = 0.004$), layer 4 swellings being smaller than those of layers 1–3 ($p = 0.021$) and layer 5a ($p = 0.044$). The layer by layer comparisons of these size distributions show that there is a very highly significant difference for all layers pairwise comparisons between S1BF and V1 (Kolmogorov–Smirnov tests, $p < 0.001$). The size distributions for each layers for the stereological sampling (Fig. 7D), clearly show that axonal swellings in V1 are smaller than those in S1BF. The size distributions of swellings for each layers in the reconstructed axons (Fig. 7C) and in the stereological sampling (Fig. 7D), clearly show a greater asymmetry towards the right in S1BF that in V1.

Discussion

The aim of this study was to describe the structure of the reciprocal connections between visual and somatosensory cortices in the mouse. We show that the primary visual cortex and the barrel field of the primary somatosensory cortex of C57Bl/6J mice are linked by direct reciprocal connections. This supports visuotactile interactions at the initial stage of sensory processing in primary sensory cortices. We extend these findings by showing a significant asymmetry of the strength and of the axonal morphology of these reciprocal connections. The projection from V1 to S1 is predominantly to the barrel field and stronger than the reciprocal projection to V1. We also demonstrate that these connections between primary sensory cortices do not fit in the classification scheme of feedforward and feedback cortical projections. Finally, axons in the projection from V1 to S1BF were thicker and had some large anterogradely labeled axonal swellings not found in the projection from S1BF to V1, suggesting a greater importance of Class 1B glutamatergic inputs from the visual cortex to the somatosensory cortex. This asymmetry suggests that, in the mouse, the visual projection to the primary somatosensory cortex has a greater driving influence on the somatosensory cortex than the reciprocal projection from the somatosensory cortex to the visual cortex.

Direct Reciprocal Projection Between Visual and Somatosensory Cortices

Numerous retrogradely labeled neuronal cell bodies were found in V1 and S1 following injections in S1BF and V1 respectively. The projection from V1 to S1BF was more robust than previously shown (Campi et al. 2010; Wang et al. 2012). The projection from the somatosensory to the visual cortex was significant as previously shown in the mouse (Charbonneau et al. 2012; Wang et al. 2012; Stehberg et al. 2014; Zingg et al. 2014), rat (Sieben et al. 2013; Stehberg et al. 2014; Zakiewicz et al. 2014), and gerbil (Henschke et al. 2014).

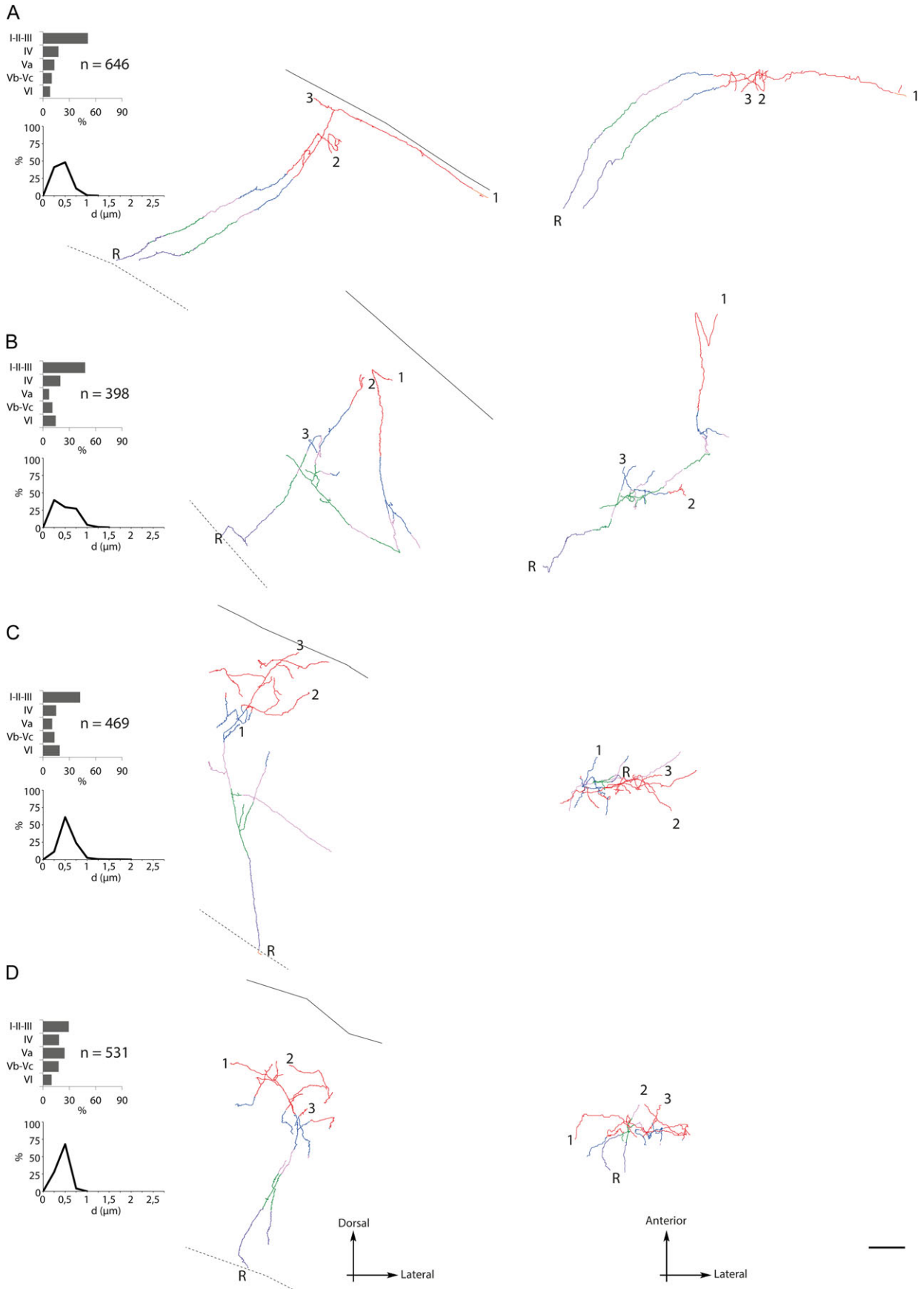

Figure 5. Single axons in V1 following an injection of BDA in S1BF of C57Bl/6 J mice. Legends as in Figure 4.

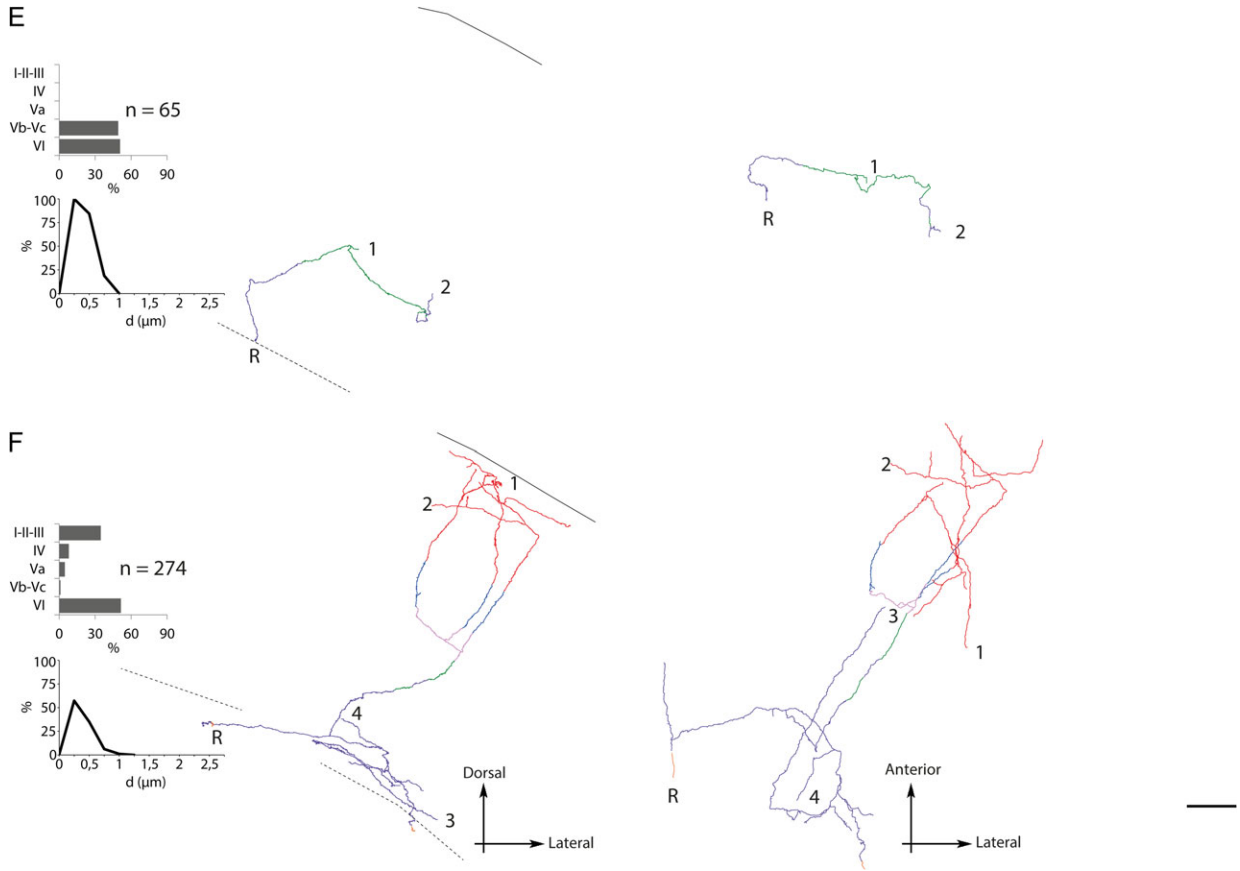

Figure 5. *Continued.*

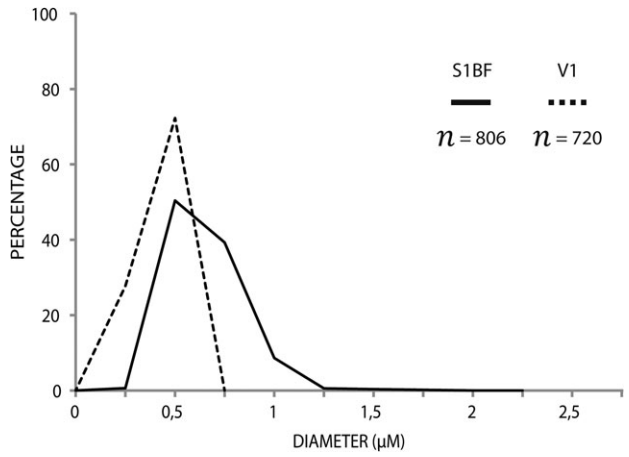

Figure 6. Size distribution of axonal diameters in S1BF (solid line) following BDA injections in V1 and in V1 following injections in S1BF (dotted line). *n* = the number of counted axons for each projection.

Direct projections between primary sensory areas are sparse in primates (Falchier et al. 2002; Rockland and Ojima 2003; Clavagnier et al. 2004; Cappe and Barone 2005; Cappe et al. 2009). The greater importance of direct interactions between primary sensory cortices in rodents than in primates could indicate a greater reliance of multisensory processing on low-level cortices than on top down feedback projections from higher level multisensory cortices as in primates. The involvement of the direct connections between primary sensory cortices in cross-modal interactions has been demonstrated in rodents (Iurilli et al. 2012; Sieben et al. 2013; Sieben et al. 2015). Top down projections to primary sensory cortices from other sensory modalities and non–sensory cortices are nonetheless present and diverse in rodents (Miller and Vogt 1984; Paperna and Malach 1991; Budinger et al. 2006; Budinger and Scheich 2009; Charbonneau et al. 2012; Zingg et al. 2014) and there is direct evidence for a contribution of top down feedback to the primary visual cortex form association cortices in the mouse (Hirokawa et al. 2008; Yoshitake et al. 2013) and transthalamic pathways (Sieben et al. 2013) in multisensory processing. The relative contribution of direct connections between primary sensory areas and of feedback projections from association cortical areas in multisensory processing is still an open question.

Hierarchical Order of Primary Sensory Cortices

The layer indices obtained from the number of retrogradely labeled neurons in supra- and infragranular layers show that the connection of the somatosensory cortex to the visual cortex has features of a feedback projection that is reciprocated by a lateral projection from the visual cortex. This asymmetry suggests that these two primary sensory cortices might not be at the same hierarchical level in the cortical network. Indeed, the asymmetry of reciprocal connections between cortical areas is the basis for establishing hierarchical levels in the cortex (Rockland and Pandya 1979; Felleman and Van Essen 1991; Coogan and Burkhalter 1993; Hilgetag et al. 2000; Markov et al. 2014). Negative layer indices, typical of feedback cortical projections, have also been demonstrated in the mouse projection of

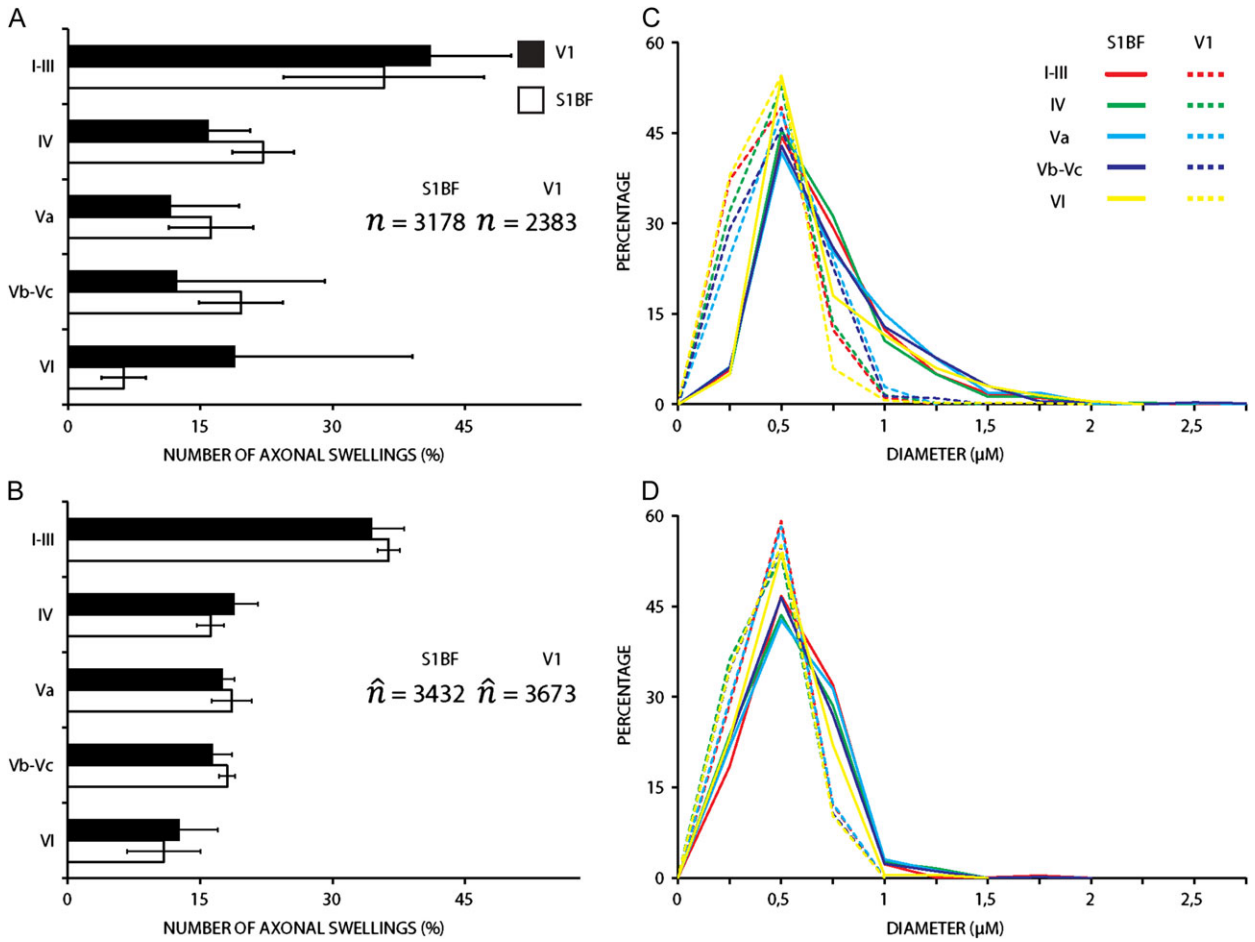

Figure 7. Laminar and size distribution of axonal swellings in S1BF and V1 following an injection of BDA in V1 cortex and S1BF respectively of C57Bl/6 J mice from the sample of reconstructed single axons (*A* and *C* resp) and from the stereological sampling of these cortical areas following columnar BDA cortical injections (*B* and *D* resp). Solid lines correspond to layers in S1BF and dotted lines correspond to layers in V1 (*C*/*D*). $\hat{n}$ = the number of swellings estimated by the stereological sampling. n = the total number of swellings measured in the stereological sampling scheme.

somatosensory cortex to V1 (Charbonneau et al. 2012). In the gerbil, the connection from somatosensory to primary visual cortex also has features of a feedback projection, whereas the reciprocal connection has those of a lateral projection (Henschke et al. 2014). One study in the rat however, shows more numerous retrogradely labeled neurons in the supragranular layers of V1 following tracer injections in somatosensory cortex suggesting a feedforward projection (Sieben et al. 2013). In the gerbil, as we have also shown in the mouse (Charbonneau et al. 2012), V1 receives feedback projections from both the primary auditory and somatosensory cortices. In the gerbil, these projections are reciprocated by a feedforward projection to the auditory cortex and a lateral projection to the somatosensory cortex, and the auditory and somatosensory cortices are reciprocally linked by lateral projections (Henschke et al. 2014). This suggests that primary somatosensory and auditory cortices would be higher in the cortical hierarchy than V1, and possibly at similar levels.

Primary sensory cortices, are the initial portals to cortical networks for specific sensory modalities, and could have been expected to stand at the same hierarchical level and linked by symmetric lateral connections. This is clearly not the case. It is generally believed that in hierarchical cortical networks, a descending pathway is, reciprocated by an ascending projection, and if one is lateral, its counterpart should also be lateral (Felleman and Van Essen 1991). It has been suggested that the hierarchical organization of cortical areas in the rat could be based on half steps in that a feedback projection could be reciprocated by a lateral type projection (Coogan and Burkhalter 1993). Such half steps were not reported in primates, in which feedback projections are strictly paired with feedforward projections (Coogan and Burkhalter 1993). The use of continuous indices such as the layer indices used here, have shown that the cortical areas are not ranked in the cortical hierarchical structure in discrete steps but in a continuum of levels (Vezoli et al. 2004; Markov et al. 2014).

The laminar distribution of anterogradely labeled terminals demonstrates that both projections between V1 and S1BF have features of feedback projections as shown by the dense terminal labeling in both supra- and infragranular layers and by the much lighter labeling in layer 4 (Coogan and Burkhalter 1990, 1993). Indeed, in rodents, feedback projections target both supra- and infragranular layers generally avoiding layer 4 whereas feedforward projections target all cortical layers (Coogan and Burkhalter 1990, 1993). Whether this terminal labeling in layer 4 is a specific attribute of projections between primary sensory cortices is not known. There are no quantitative assessments of the laminar distribution of axonal swellings in cortical projections in rodents showing the absence of layer 4 labeling in feedback projections. We provide here a first quantitative evaluation of the laminar distribution of axonal

swellings in corticocortical projections between primary sensory cortices, and show significant terminal labeling in layer 4. Moreover, single axon reconstructions also show axonal branching in layer 4 in both projections. This terminal labeling is quite different to what is seen in feedback projections in primates that target mainly superficial cortical layers. There are no accounts of terminal structure of projections between primary sensory cortices in primates.

In the projection from the somatosensory barrel field to V1, the laminar distribution of retrogradely labeled neurons in the barrel field and the terminal labeling in V1 both indicate that this projection has features of a feedback projection type. However, in the projection from the visual cortex to the barrel field, the retrograde labeling and the terminal labeling are not strictly consistent with a feedback or feedforward types of projections. The laminar distribution of terminals in the barrel field is the same as the one in V1 and suggests a feedback projection whereas the laminar distribution of retrogradely labeled neurons yields layer indices close to 0 suggesting a lateral type projection. This could be particular to projections between primary sensory cortices and could also indicate that a dichotomous classification of cortical projections in feedforward and feedback types is not appropriate to describe all possibilities.

Asymmetry of the Strength of the Reciprocal Projections Between V1 and S1BF

Retrograde transport of cholera toxin showed a stronger projection from V1 to S1BF than from S1 and S1BF to V1. Similarly, a strong projection of the visual cortex to the somatosensory cortex and a moderate reciprocal projection have been shown in the gerbil (Henschke et al. 2014). In the gerbil, the primary visual cortex has the strongest multisensory inputs receiving similar moderate inputs from the primary auditory and somatosensory cortices. On the other hand, the somatosensory cortex receives a strong input from the visual cortex but only a faint input from the auditory cortex. The primary auditory cortex receives only faint inputs from the other primary sensory cortices (Henschke et al. 2014). These observations suggest that the mutual influences between the senses are not equivalent in strength. In the mouse, as in the gerbil, the influence of the visual cortex on the somatosensory cortex would be the stronger one.

A functional asymmetric reciprocity has also been shown between primary visual and somatosensory cortices in the mouse. Visual stimulation produces a small subthreshold depolarization of layer 2/3 neurons of the somatosensory cortex whereas whisker deflection hyperpolarizes neurons in these layers by direct corticocortical recruiting of local translaminar inhibitory circuits (Iurilli et al. 2012).

Size of Axonal Swellings

The asymmetry of the reciprocal projections between V1 and S1BF is also seen in the size distribution of axonal swellings. All cortical layers in S1BF had some larger swellings not seen in V1. The size distributions we obtained here are commensurate with those reported in the reciprocal connections between primary and secondary auditory cortices in mice (Covic and Sherman 2011). Class 1B synapses are anatomically correlated with larger synaptic terminals and Class 2 synapses with smaller synaptic terminals (Covic and Sherman 2011; see Sherman and Guillery 2013a). We surmise that the larger swellings in the projection from V1 to S1BF in our results, reflects a greater proportion of Class 1 terminals therein and that the large population of smaller swellings, which appears to be predominant in both projections, could be Class 2 terminals.

In thalamocortical and corticothalamic pathways, Class 1B and 2 are respectively considered drivers and modulators (Sherman and Guillery 1996, 1998; Reichova and Sherman 2004; Lee and Sherman 2008, 2009a, 2009b; Viaene et al. 2011; Petrof and Sherman 2013). This model of glutamatergic transmission predicts that information flow depends on Class 1 pathways (Covic and Sherman 2011; Sherman and Guillery 2013a). If this is the case, our results would indicate that visual information is transmitted to the somatosensory cortex while tactile information can mostly modulate activity in the visual cortex.

The presence of larger terminals in S1BF not found in V1 would indicate that V1 might exert a driving influence on the somatosensory cortex that is not reciprocated in its projection back to the visual cortex. This asymmetry could reflect the greater influence of vision on whisker mediated tactile sensing and navigation in mice, and the relative importance of the different senses in rodents, which rely less on visual stimuli compared with the more visual carnivores and primates (Whishaw and Kolb 2004). Moreover, the benefit of multisensory interactions is larger for some modalities (Hollensteiner et al. 2015). The modality precision hypothesis states that the resolution of intersensory discrepancies will be in favor of the more precise of the two modalities (see Welch and Warren 1986 for review and references). This theory is based on an order of dominance between sensory modalities derived from their respective spatial precision. Whisker mediated tactile sensing is spatially more precise than vision in rats and mice, tactile acuity greatly surpassing their visual discrimination capabilities (Carvell and Simons 1990; Prusky et al. 2000; Wu et al. 2013). The presence of the larger presumed Class 1 terminals in the projection from the visual cortex to the barrel field would suggest that the visual cortex provides the somatosensory cortex with more specific visual information than the reciprocal projection of S1BF to V1. Indeed, Class 1 responses are mediated by ionotropic receptors which exhibit fast postsynaptic response dynamics compared with the much slower Class 2 metabotropic mediated responses. Class 1B inputs will therefore maintain the highly specific temporal attributes of the conveyed information (see Sherman and Guillery 2013a). In visuotactile integration, the less precise visual information will contribute in providing additional information to the somatosensory cortex through a stronger driving projection. The absence of larger terminals in the projection from the barrel field to the visual cortex suggests that it has more modulatory influence on visual cortex activity. This could indicate that in the mouse, vision is more important to enhance the context of whisking and that tactile information is not as important for the enhancement of visual information.

It is noteworthy that there are very few larger swellings in the visual cortex projection to the barrel field. This is also observed in many other cortical and subcortical pathways. Even though Class 1 inputs are considered as the main information carriers in thalamic circuits, it is common that they are vastly outnumbered by Class 2 inputs, accounting for less than 10% of the total number of synapses in thalamus, with some estimates putting them as low as 2% (Van Horn et al. 2000; Wang et al. 2002; Huppé-Gourgues et al. 2006). Retinogeniculate projections are considered as Class 1 inputs and are functionally the dominant input to geniculate neurons however they account for only 5% of geniculate synapses whereas cortical inputs account for 30–40% of synapses therein (Erisir et al. 1998; Van Horn et al. 2000). We cannot evaluate the proportions of terminals that could be assigned to these functional classes having no basis for determining a

cut-off size as a reliable criterion for such a classification. However, we do provide the first quantitative unbiased stereological sampling of axonal swellings laminar and size distributions in a cortical connection. This sampling clearly shows that small terminals, that would most likely have Class 2 properties, largely outnumber the larger terminals.

In the projection from V1 to S1BF, there were no significant differences of the size distributions of axonal swellings between layers. This pattern is different than what was reported in the corticocortical connection between auditory (Covic and Sherman 2011) and visual cortices (De Pasquale and Sherman 2011). In the reciprocal connection between primary and secondary auditory cortices, layers 5a and 6 received almost only Class 2 inputs whereas layer 5b received almost only Class 1B inputs. This was correlated with anatomical observations showing significantly smaller terminals in layers 4 and 5b than in layers 5a and 6 (Covic and Sherman 2011). We show here that there is a wide range of terminal sizes in the supragranular layers in the somatosensory cortex that would support the presence of the two types of postsynaptic responses. Conversely, in the projection from S1BF to V1, the swellings in layer 4 were smaller than those in the bottom tiers of layer 5. Whether this indicates a greater contribution of Class 1 inputs therein is possible, but very large terminals were not observed in this projection to the somatosensory cortex.

Single Axon Morphology

This is the only account of single axon morphology of interareal connections between primary sensory cortices. Although we have here only small samples of axons, significant observations can be drawn from these. There is a diversity of morphologies in both projections, supporting previous studies in showing that a single cortical projection likely comprises several morphofunctional conduction channels (see Rockland 2015 for further references and discussion). This is further supported by the diversity in the laminar distribution of terminals for each of these axons. The overall laminar distribution of terminals results from the sum of individual axons that have very different terminal arbor structures. Axonal morphologies exhibit a mosaic of features. Some axons had terminal arbors that form a more or less defined columnar projection with a limited tangential spread, whereas others were widely divergent over large distances. Some axons show both features. These are not typical of axons in cortical feedforward and feedback projections in monkeys. In general, feedforward axons have a more focused structure whereas feedback axons appear to travel greater distances and cross functional domains such as ocular dominance columns (see Rockland 2002 for review). Such a mixture of columnar and divergent features could be particular to connections between primary sensory cortices or can also be related to the less-modular, salt-and-pepper organisation of the mouse cortex. The more divergent axons seen here were in the projection from V1 to the barrel field and would likely target more than one barrel.

In corticothalamic projections there are two very distinct types of axons (see Sherman and Guillery 2013b for extended discussion). Thick axons originate from layer 5 pyramidal neurons and bear type II axon terminals that convey Class 1 inputs. Thin axons are issued by neurons of layer 6 and bear type I axon terminals that convey Class 2 inputs (Bourassa and Deschenes 1995; Bourassa et al. 1995; Sherman and Guillery 2013a). There is no evidence here for corticocortical axons with exclusively large terminals similar to the thick corticothalamic axons issued by layer 5 neurons. There are several reconstructed axons in our sample that bear only very small terminals and axon on which a wider range of terminal sizes occur. On these particular axons, again very small terminals largely outnumber the larger ones. This might indicate two distinct types of axons on the basis of the presence of some larger terminals.

Axons entering the somatosensory barrel field were significantly thicker than the axons entering the primary visual cortex. Moreover in S1BF there were a few quite thick axons that were never observed in the projection to the visual cortex, further supporting the asymmetric projections between the two primary sensory cortices. Previous studies in primates have shown that corticofugal axons originating from different cortical areas have different diameters whereas the thickness of axons of inter-area connections were not different (Tomasi et al. 2012). Another study showed that corticocortical projections to different targets may have axons of different diameters (Innocenti et al. 2014). Our results show here that both projections comprise mainly a population of quite thin axons with the projection to the visual cortex having the thinner axons and that the projection of S1BF to the visual cortex contains a few larger caliber axons. Axonal diameter is related to conduction speeds. Therefore, we might expect that the projection from the somatosensory barrel field is more homogeneous in this respect than the projection from the visual cortex to the barrel field. The greater range in axon diameters in the projection to the barrel field supports the idea that a single connection can be a complex channel comprising a range of parallel axonal pathways that might generate different conduction delays (Innocenti et al. 2014).

Conclusions

This study shows a direct and reciprocal connection of lateral type from V1 to S1BF and of feedback type from S1BF to V1. This direct link between the visual cortex and the barrel field further supports the notion that primary sensory cortices integrate multisensory inputs. This study indicates that these heteromodal connections between low-level primary sensory cortices although reciprocal, are certainly not symmetrical. This reciprocal connection between the visual cortex and the barrel field could be the anatomical substrate of the influence of vision on tactile sensing and navigation by the whiskers in mice. We show here that the reciprocal connection between the visual and somatosensory cortex of the mouse would be a good experimental model for the study of functional and behavioral asymmetries between sensory modalities.

Funding

Discovery grants of the Natural Sciences and Engineering Research Council of Canada (NSERC) to D.B. and G.B., and the Canadian Foundation for Innovation to D.B. S.R. was supported by an NSERC undergraduate student award.

Notes

We are grateful to Nadia Desnoyers for animal care and maintenance. Contributions from UQTR are also acknowledged. *Conflict of Interest*: None declared.

References

Berezovskii VK, Nassi JJ, Born RT. 2011. Segregation of feedforward and feedback projections in mouse visual cortex. J Comp Neurol. 18:3672–3683.

Bizley JK, King AJ. 2009. Visual influences on ferret auditory cortex. Hear Res. 258:55–63.

Bizley JK, Nodal FR, Bajo VM, Nelken I, King AJ. 2007. Physiological and anatomical evidence for multisensory interactions in auditory cortex. Cereb Cortex. 17:2172–2189.

Bourassa J, Deschenes M. 1995. Corticothalamic projections from the primary visual cortex in rats: a single fiber study using biocytin as an anterograde tracer. Neuroscience. 66:253–263.

Bourassa J, Pinault D, Deschenes M. 1995. Corticothalamic projections from the cortical barrel field to the somatosensory thalamus in rats: a single-fibre study using biocytin as an anterograde tracer. Eur J Neurosci. 7:19–30.

Brosch M, Selezneva E, Scheich H. 2005. Nonauditory events of a behavioral procedure activate auditory cortex of highly trained monkeys. J Neurosci. 29:6797–6806.

Budinger E, Heil P, Hess A, Scheich H. 2006. Multisensory processing via early cortical stages: connections of the primary auditory cortical field with other sensory systems. Neuroscience. 143:1065–1083.

Budinger E, Laszcz A, Lison H, Scheich H, Ohl FW. 2008. Non-sensory cortical and subcortical connections of the primary auditory cortex in Mongolian gerbils: bottom-up and top-down processing of neuronal information via field AI. Brain Res. 1220:2–32.

Budinger E, Scheich H. 2009. Anatomical connections suitable for the direct processing of neuronal information of different modalities via the rodent primary auditory cortex. Hear Res. 258:16–27.

Campi KL, Bales KL, Grunewald R, Krubitzer L. 2010. Connections of auditory and visual cortex in the prairie vole (Microtus ochrogaster): evidence for multisensory processing in primary sensory areas. Cereb Cortex. 20:89–108.

Cappe C, Rouiller EM, Barone P. 2009. Multisensory anatomical pathways. Hear Res. 258:28–36.

Cappe C, Barone P. 2005. Heteromodal connections supporting multisensory integration at low levels of cortical processing in the monkey. Eur J Neurosci. 22:2886–2902.

Carvell GE, Simons DJ. 1990. Biometric analyses of vibrissal tactile discrimination in the rat. J Neurosci. 10:2638–2648.

Caviness VS. 1975. Architectonic map of neocortex of the normal mouse. J Comp Neurol. 164:247–263.

Charbonneau V, Laramée ME, Boucher V, Bronchti G, Boire D. 2012. Cortical and subcortical projections to primary visual cortex in anophthalmic, enucleated and sighted mice. Eur J Neurosci. 7:2949–2963.

Clavagnier S, Falchier A, Kennedy H. 2004. Long-distance feedback projections to area V1: implications for multisensory integration, spatial awareness, and visual consciousness. Cogn Affect Behav Neurosci. 2:117–126.

Coogan TA, Burkhalter A. 1990. Conserved patterns of cortico-cortical connections define areal hierarchy in rat visual cortex. Exp Brain Res. 80:49–53.

Coogan TA, Burkhalter A. 1993. Hierarchical organization of areas in rat visual cortex. J Neurosci. 13:3749–3772.

Covic EN, Sherman SM. 2011. Synaptic properties of connections between the primary and secondary auditory cortices in mice. Cereb Cortex. 21:2425–2441.

De Pasquale R, Sherman SM. 2011. Synaptic properties of corticocortical connections between the primary and secondary visual cortical areas in the mouse. J Neurosci. 31:16494–16506.

Driver J, Noesselt T. 2008. Multisensory interplay reveals crossmodal influences on 'sensory-specific' brain regions, neural responses, and judgments. Neuron. 57:11–23.

Erisir A, Van Horn SC, Sherman SM. 1998. Distribution of synapses in the lateral geniculate nucleus of the cat: differences between laminae A and A1 and between relay cells and interneurons. J Comp Neurol. 390:247–255.

Ernst MO, Bulthoff HH. 2004. Merging the senses into a robust percept. Trends Cogn Sci. 8:162–169.

Falchier A, Cappe C, Barone P., Schroeder CE. 2013.Sensory convergence in low-level cortices. In: Stein BE, editor. The new handbook of multisensory processing. Cambridge, MA, London, England: The MIT Press. p. 67–79.

Falchier A, Clavagnier S, Barone P, Kennedy H. 2002. Anatomical evidence of multimodal integration in primate striate cortex. J Neurosci. 22:5749–5759.

Felleman DJ, Van Essen DC. 1991. Distributed hierarchical processing in the primate cerebral cortex. Cereb Cortex. 1:1–47.

Foxe JJ, Morocz IA, Murray MM, Higgins BA, Javitt DC, Schroeder CE. 2000. Multisensory auditory-somatosensory interactions in early cortical processing revealed by high-density electrical mapping. Brain Res Cogn Brain Res. 10:77–83.

Franklin, BJ, Paxinos, G. 2008. The Mouse Brain in Stereotaxic Coordinates. San Diego: Academic Press.

Ghazanfar AA, Schroeder CE. 2006. Is neocortex essentially multisensory?. Trends Cogn Sci. 10:278–285.

Giard MH, Peronnet F. 1999. Auditory-visual integration during multimodal object recognition in humans: a behavioral and electrophysiological study. J Cogn Neurosci. 11:473–490.

Godement P, Saillour P, Imbert M. 1979. Thalamic afferents to the visual cortex in congenitally anophthalmic mice. Neurosci Lett. 13:271–278.

Gonchar Y, Burkhalter A. 1999. Differential subcellular localization of forward and feedback interareal inputs to parvalbumin expressing GABAergic neurons in rat visual cortex. J Comp Neurol. 406:346–360.

Gonchar Y, Burkhalter A. 2003. Distinct GABAergic targets of feedforward and feedback connections between lower and higher areas of rat visual cortex. J Neurosci. 23:10904–10912.

Henschke JU, Noesselt T, Scheich H, Budinger E. 2014. Possible anatomical pathways for short-latency multisensory integration processes in primary sensory cortices. Brain Struct Funct. 220:955–977.

Hilgetag CC, O'Neill MA, Young MP. 2000. Hierarchical organization of macaque and cat cortical sensory systems explored with a novel network processor. Philos Trans R Soc Lond B Biol Sci. 355:71–89.

Hirokawa J, Bosch M, Sakata S, Sakurai Y, Yamamori T. 2008. Functional role of the secondary visual cortex in multisensory facilitation in rats. Neuroscience. 153:1402–1417.

Hishida R, Kudoh M, Shibuki K. 2014. Multimodal cortical sensory pathways revealed by sequential transcranial electrical stimulation in mice. Neurosci Res. 87:49–55.

Hollensteiner KJ, Pieper F, Engler G, Konig P, Engel AK. 2015. Crossmodal integration improves sensory detection thresholds in the ferret. PLoS One. 10:e0124952.

Huppé-Gourgues F, Bickford ME, Boire D, Ptito M, Casanova C. 2006. Distribution, morphology, and synaptic targets of corticothalamic terminals in the cat lateral posterior-pulvinar complex that originate from the posteromedial lateral suprasylvian cortex. J Comp Neurol. 497:847–863.

Innocenti GM, Vercelli A, Caminiti R. 2014. The diameter of cortical axons depends both on the area of origin and target. Cereb Cortex. 24:2178–2188.

Iurilli G, Ghezzi D, Olcese U, Lassi G, Nazzaro C, Tonini R, Tucci V, Benfenati F, Medini P. 2012. Sound-driven synaptic inhibition in primary visual cortex. Neuron. 73:814–828.

Kaas JH., Collins CE. 2013.The resurection of multisensory cortex in primates: connection patterns that integrate modalities. In: Calvert GA, Spence C, Stein BE editors. The handbook of multisensory processes. Cambridge: The MIT Press. p. 285–293.

Laurienti PJ, Burdette JH, Wallace MT, Yen YF, Field AS, Stein BE. 2002. Deactivation of sensory-specific cortex by cross-modal stimuli. J Cogn Neurosci. 14:420–429.

Lee CC, Sherman SM. 2008. Synaptic properties of thalamic and intracortical inputs to layer 4 of the first- and higher-order cortical areas in the auditory and somatosensory systems. J Neurophysiol. 100:317–326.

Lee CC, Sherman SM. 2009a. Glutamatergic inhibition in sensory neocortex. Cereb Cortex. 19:2281–2289.

Lee CC, Sherman SM. 2009b. Modulator property of the intrinsic cortical projection from layer 6 to layer 4. Front Syst Neurosci. 3:3.

Macaluso E. 2006. Multisensory processing in sensory-specific cortical areas. Neuroscientist. 12:327–338.

Markov NT, Vezoli J, Chameau P, Falchier A, Quilodran R, Huissoud C, Lamy C, Misery P, Giroud P, Ullman S, et al. 2014. Anatomy of hierarchy: feedforward and feedback pathways in macaque visual cortex. J Comp Neurol. 522:225–259.

Miller MW, Vogt BA. 1984. Direct connections of rat visual cortex with sensory, motor, and association cortices. J Comp Neurol. 226:184–202.

Paperna T, Malach R. 1991. Patterns of sensory intermodality relationships in the cerebral cortex of the rat. J Comp Neurol. 308:432–456.

Petrof I, Sherman SM. 2013. Functional significance of synaptic terminal size in glutamatergic sensory pathways in thalamus and cortex. J Physiol. 591:3125–3131.

Prusky GT, West PW, Douglas RM. 2000. Behavioral assessment of visual acuity in mice and rats. Vision Res. 40:2201–2209.

Reichova I, Sherman SM. 2004. Somatosensory corticothalamic projections: distinguishing drivers from modulators. J Neurophysiol. 92:2185–2197.

Rockland KS. 2002. Visual cortical organization at the single axon level: a beginning. Neurosci Res. 42:155–166.

Rockland KS. 2015. About connections. Front Neuroanat. 9:61.

Rockland KS, Ojima H. 2003. Multisensory convergence in calcarine visual areas in macaque monkey. Int J Psychophysiol. 50:19–26.

Rockland KS, Pandya DN. 1979. Laminar origins and terminations of cortical connections of the occipital lobe in the rhesus monkey. Brain Res. 179:3–20.

Schroeder CE, Smiley J, Fu KG, McGinnis T, O'Connell MN, Hackett TA. 2003. Anatomical mechanisms and functional implications of multisensory convergence in early cortical processing. Int J Psychophysiol. 50:5–17.

Sherman SM, Guillery RW. 1996. Functional organization of thalamocortical relays. J Neurophysiol. 76:1367–1395.

Sherman SM, Guillery RW. 1998. On the actions that one nerve cell can have on another: distinguishing "drivers" from "modulators". Proc Natl Acad Sci USA. 95:7121–7126.

Sherman SM, Guillery RW. 2013a.Functional connections of cortical areas. Cambridge (MA), London, England: MIT Press.

Sherman SM, Guillery RW. 2013b. Functional connections of cortical areas A new view from the thalamus. Cambridge, Massachussetts; London, England: MIT Press.

Sieben K, Bieler M, Roder B, Hanganu-Opatz IL. 2015. Neonatal restriction of tactile inputs leads to long-lasting impairments of cross-modal processing. PLoS Biol. 13:e1002304.

Sieben K, Roder B, Hanganu-Opatz IL. 2013. Oscillatory entrainment of primary somatosensory cortex encodes visual control of tactile processing. J Neurosci. 33:5736–5749.

Stehberg J, Dang PT, Frostig RD. 2014. Unimodal primary sensory cortices are directly connected by long-range horizontal projections in the rat sensory cortex. Front Neuroanat. 8:93.

Stein BE, Meredith MA. 1993. The merging of the senses. Cambridge, Massachusetts: MIT Press.

Stein BE, Stanford TR. 2008. Multisensory integration: current issues from the perspective of the single neuron. Nat Rev Neurosci. 2008/03/21:255–266.

Tomasi S, Caminiti R, Innocenti GM. 2012. Areal differences in diameter and length of corticofugal projections. Cereb Cortex. 22:1463–1472.

Van Horn SC, Erisir A, Sherman SM. 2000. Relative distribution of synapses in the A-laminae of the lateral geniculate nucleus of the cat. J Comp Neurol. 416:509–520.

Vezoli J, Falchier A, Jouve B, Knoblauch K, Young M, Kennedy H. 2004. Quantitative analysis of connectivity in the visual cortex: extracting function from structure. Neuroscientist. 10:476–482.

Viaene AN, Petrof I, Sherman SM. 2011. Synaptic properties of thalamic input to layers 2/3 and 4 of primary somatosensory and auditory cortices. J Neurophysiol. 10:279–292.

Wang Q, Burkhalter A. 2007. Area map of mouse visual cortex. J Comp Neurol. 502:339–357.

Wang Q, Sporns O, Burkhalter A. 2012. Network analysis of corticocortical connections reveals ventral and dorsal processing streams in mouse visual cortex. J Neurosci. 32:4386–4399.

Wang S, Eisenback MA, Bickford ME. 2002. Relative distribution of synapses in the pulvinar nucleus of the cat: implications regarding the "driver/modulator" theory of thalamic function. J Comp Neurol. 454:482–494.

Welch RB, Warren DH. 1986. Intersensory interactions. In: Boff KR, Kaufman L, Thomas JP, editor. Handbook of perception and human performance. New York: J. Wiley. pp. 25-1–25-36.

West MJ, Gundersen HJ. 1990. Unbiased stereological estimation of the number of neurons in the human hippocampus. J Comp Neurol. 296:1–22.

West MJ, Slomianka L, Gundersen HJ. 1991. Unbiased stereological estimation of the total number of neurons in thesubdivisions of the rat hippocampus using the optical fractionator. Anat Rec. 231:482–497.

Whishaw IQ, Kolb B. 2004. The behavior of the laboratory rat: a handbook with tests. USA: Oxford University Press.

Wu HP, Ioffe JC, Iverson MM, Boon JM, Dyck RH. 2013. Novel, whisker-dependent texture discrimination task for mice. Behav Brain Res. 237:238–242.

Yamashita A, Valkova K, Gonchar Y, Burkhalter A. 2003. Rearrangement of synaptic connections with inhibitory neurons in developing mouse visual cortex. J Comp Neurol. 464:426–437.

Yoshitake K, Tsukano H, Tohmi M, Komagata S, Hishida R, Yagi T, Shibuki K. 2013. Visual map shifts based on whisker-guided cues in the young mouse visual cortex. Cell Rep. 5: 1365–1374.

Zakiewicz IM, Bjaalie JG, Leergaard TB. 2014. Brain-wide map of efferent projections from rat barrel cortex. Front Neuroinform. 8:5.

Zingg B, Hintiryan H, Gou L, Song MY, Bay M, Bienkowski MS, Foster NN, Yamashita S, Bowman I, Toga AW, et al. 2014. Neural networks of the mouse neocortex. Cell. 156: 1096–1111.